A Theoretical and Experimental Study of the CN + NO Association Reaction

Stephen J. Klippenstein*

Chemistry Department, Case Western Reserve University, Cleveland, Ohio 44106-7078

D. L. Yang, T. Yu, S. Kristyan, and M. C. Lin*

Chemistry Department, Emory University, Atlanta, Georgia 30322-1400

S. H. Robertson

Molecular Simulations Inc., 240/250, The Quorum, Barnwell Road, Cambridge CB5 8RE, U.K.

Received: April 22, 1998; In Final Form: June 26, 1998

A pulsed-laser photolysis/laser-induced fluorescence technique is employed in the determination of the pressure and temperature dependence of the reaction of CN with NO in the range from 207 to 740 K and for Ar bath gas pressures ranging from 30 to 900 Torr. A variational RRKM model coupled with a one-dimensional master equation treatment provides a reasonably satisfactory description of the available kinetic data for both the association and dissociation processes. The association kinetic data is best fit by a collisional energy transfer parameter, $\langle \Delta E \rangle_{down}$, for the simple exponential down model, which gradually increases from −35 cm^{-1} at 100 K to −500 cm^{-1} at 740 K. The expression 3.4×10^{-10} exp(120/*T*) cm^3 s^{-1} reproduces the present theoretical estimates for the high-pressure rate constant in the range from 207 to 740 K.

I. Introduction

The CN radical is an important reactive species in the combustion of [H,C,N,O]-containing nitramine propellants[1−3] and is relevant to the NO_x chemistry in hydrocarbon combustion processes.[4,5] The reaction of CN with NO has been shown to dominate the combustion of RDX (cyclotrimethylenetrinitramine) in its late stages because of the stabilities of the two radical species.

At low temperatures, the reaction of CN with NO is believed to occur primarily by the association process producing NCNO with strong pressure dependence.[6,7] This process is directly related to the photodissociation reaction of NCNO, investigated extensively by Wittig, by Zewail, and their co-workers.[8,9] These state-of-the-art experiments provided wide-ranging results for the energy dependence of both the product rovibronic state distributions[8] and the total rate constants.[9] In previous work we demonstrated that variational RRKM theory employing a qualitatively realistic model potential provides a satisfactory description of both the product state distributions and rate constants for the dissociation of NCNO.[10]

In this work, new experimental results are presented for the temperature and pressure dependence of the association of CN with NO. Comparison is then made with a slightly revised version of the variational RRKM model of ref 10. In the theoretical analysis the pressure dependence is treated via a one-dimensional master equation employing the simple exponential down model for the energy dependence of the transfer coefficients. In related work, Sims and Smith have recently studied this association process at a complementary set of *T* and *P*, which corresponds to the low-*P* and low-*T* range of the present experimental study.[7] Comparisons with these data are also made herein.

The experimental and theoretical methodologies employed in the present work are summarized in sections II and III, respectively. The experimental and theoretical results are then presented and discussed in section IV, with some concluding remarks provided in section V.

II. Experimental Section

The pulsed-laser photolysis/laser-induced fluorescence (PLP/LIF) technique employed in the present study has been described in our previous publications.[6,11] The kinetic measurements were carried out in a Pyrex reaction cell with two oppositely mounted side arms. For the study above room temperature, the reactor was resistively heated and the temperature was controlled to within 1 K. For the study below room temperature, a similar reactor with cooling jacket for circulation of a coolant (i.e., methanol with dry ice cooling) was employed. The reaction was measured at four temperatures between 207 and 740 K.

The CN radical was generated by the photolysis of ICN at 248 nm using a KrF excimer laser (Lambda Physik LPX105). The production and decay of the radical were monitored by LIF using a nitrogen-laser pumped dye laser (Laser Photonics). The photodissociation laser was introduced in the reactor through one of the baffled side arms and the probing laser through the baffled, opposite side arm, overlapping with the dissociation laser at the center of the reactor. The induced red-shifted (0,1) CN fluorescence at 420 nm was collected with a photomultiplier tube (Hamamatsu 955) through a lens-band filter set from the side window perpendicular to the laser beams. The amplified LIF signal was gated and averaged with a boxcar signal averager (Stanford Research SRS 250) interfaced with a microcomputer. A pulsed delay generator (Stanford Research DG535) was used to control the delay between the dissociation and probing laser pulses, which varied from −50 to 2000 μs, with a typical 5 μs scanning step size.

The CN precursor, ICN, and the NO reactant were mixed outside the reactor through a corrugated flexible stainless steel

S1089-5639(98)01946-X CCC: $15.00
Published on Web 08/12/1998

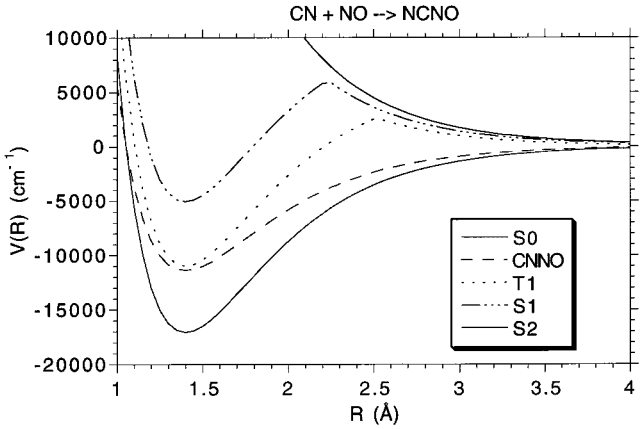

Figure 1. Schematic plot of the states involved in the association of CN with NO.

tubing and carried into the reactor with Ar. The reactant concentration was calculated by the equation [NO] = 9.66×10^{18} PF_{NO}/F_TT molecules/cm^3, where F_{NO} is the flow rate (in STP cm^3/s, STP = 273 K, 1 atm) of NO and F_T is the total flow rate. P is the reaction pressure (in Torr) measured with an MKS Baratron lead/head. T is the reaction temperature (in K) measured with a J-type thermocouple placed ≈5 mm from the collinear laser beams.

Ar (Spectra Gases, 99.9995%) and ICN (Aldrich) were used without further purification. ICN was contained in a fritted glass and carried into the reactor with the Ar carrier gas. NO (Matheson Gas Products) was purified by passing it through a dry ice-cooled $CaSO_4$ trap to remove any NO_2 impurity. The condensed NO at 77 K was distilled and used for the preparation of NO/Ar mixtures with varying compositions.

III. Computational Study

A. Ab Initio MO Calculations. A schematic plot of the states involved in the association of CN with NO is provided in Figure 1. Optimized molecular structures and vibrational frequencies were obtained for CN, NO, NCNO in the ground singlet (S_0) and triplet states (T_1), and CNNO with various electron correlation procedures, including second-order Møller Plesset perturbation theory (MP2),[12−15] configuration interaction with single and double excitations (CISD),[16−18] coupled cluster techniques incorporating single and double substitutions (CCSD),[19−24] and density functional theory[25,26] employing the Becke3−Lee−Yang−Parr (B3LYP) functional.[27] A 6-31G* basis set[12] was employed in each instance. The relative energies of these same species were obtained at the G2(MP2) level of theory.[28−30] The GAUSSIAN92/DFT quantum chemical software was employed in each of these evaluations.[31]

The molecular structures, vibrational frequencies, and relative energetics of these species are provided in Tables 1−3, respectively. Sample analyses of the transition state separating CNNO from CO + N_2 (as determined via a reaction path analysis) are also provided therein. This transition state is only of importance to the kinetics at temperatures higher than those considered here, and so the corresponding analyses were restricted to MP2/6-31G*, B3LYP/6-31G*, and G2(MP2) evaluations.

B. Kinetic Theory Background. At modest and lower temperatures the reaction of CN with NO proceeds via the formation and stabilization of an NCNO and/or CNNO complex. Indeed the G2(MP2) calculations suggest that the barrier to production of the lower energy N_2 + CO products is 7065 cm^{-1} higher than reactants. The NCNO and CNNO complexes should

TABLE 1: Molecular Structures

coordinate	MP2[a]	CISD	CCSD	B3LYP	exptl
			CN and NO[b]		
r_{CN}	1.1355	1.1558	1.1806	1.1738	1.1718
r_{NO}	1.1429	1.1465	1.1667	1.1587	1.1508
			NCNO[c]		
r_{NC}	1.1859	1.1540	1.1690	1.1658	1.163
r_{NO}	1.2407	1.1987	1.2164	1.2096	1.217
r_{CN}	1.4243	1.4259	1.4418	1.4222	1.418
θ_{NCN}	171.04	172.42	171.75	167.74	170
θ_{CNO}	112.53	112.96	112.55	115.14	113.5
			^{3}NCNO		
r_{NC}	1.1430	1.1509	1.1757	1.1796	
r_{NO}	1.1983	1.2057	1.2355	1.3057	
r_{CN}	1.3656	1.3367	1.3407	1.2279	
θ_{NCN}	177.79	175.30	174.16	172.50	
θ_{CNO}	131.28	128.91	127.27	134.70	
			CNNO		
r_{CN}	1.2042	1.1793	1.1920	1.1954	
r_{NO}	1.1905	1.1769	1.1887	1.1726	
r_{NN}	1.4997	1.4183	1.4536	1.4859	
θ_{CNN}	160.08	163.43	161.98	150.37	
θ_{NNO}	112.42	112.48	112.16	113.55	
			TS for CNNO → N_2 + CO		
r_{CN}	1.3224			1.3256	
r_{NO}	1.3261			1.3103	
r_{NN}	1.3791			1.3478	
θ_{CNN}	83.04			86.06	
θ_{NNO}	103.45			103.17	
τ_{ONNC}	35.96			31.30	

[a] Distances in Å and angles in deg. The 6-31G* basis set[1] was employed in each of the quantum chemical evaluations. [b] Experimental data from ref 32. [c] Experimental data from ref 33.

readily isomerize at energies well below their dissociation threshold. Thus, the effective bimolecular rate constant for CN reacting with NO corresponds to a thermal average of the initial rate of formation of energized complexes $k_f(E, J)$ at energy E and total angular momentum J, times the probability of collisional stabilization at each E and J.

Oftentimes a single collision does not result in the stabilization of the initially formed complex. In this case, the determination of the effective bimolecular rate constants requires the analysis of the time dependence of the populations in each E and J state, as in the master equation approach.[35] For computational simplicity a one-dimensional reduced form of the master equation is employed here, in which the J dependence of the populations is averaged over. In particular, we employ energy-dependent rate constants $k(E)$ given by the average over the thermal distribution of the complex of the E- and J-dependent rate constants $k(E, J)$. The time dependence of the populations P_i of the complex with energy E_i is then approximated as

$$\frac{dP_i}{dt} = k_c[M]\sum_j(\mathbf{R}_{ij}P_j - \mathbf{R}_{ji}P_i) - k_iP_i + \upsilon_i \qquad (1)$$

where k_c is the collision rate constant and [M] is the concentration of collider species. The first term on the right hand side of eq 1 represents the rate of transfer from state j into state i via collisions. The second term represents the corresponding rate of transfer out of state i into state j. The third term represents the rate of loss of the complex in state i due to reaction to produce separated fragments, and the last term υ_i is the source term describing the rate of reaction from NC and NO into the complex in state i.

The effective bimolecular rate constants are ultimately obtained via direct numerical inversion of the steady-state

TABLE 2: Vibrational Frequencies

mode	MP2[a]	CISD	CCSD	B3LYP	exptl
			CN and NO[b]		
CN stretch	2863	2396	2153	2162	2069
NO stretch	3913	2849	1951	1992	1904
ratio[c]	0.61(0.12)	0.77(0.09)	0.97(0.01)	0.96(0.00)	
			NCNO[d]		
CN stretch	2134	2430	2293	2277	2170
NO stretch	1405	1751	1615	1610	1501
CN stretch	873	922	874	823	820
bend 1	617	673	621	627	589
τ	300	333	292	271	270
bend 2	211	251	226	216	217
ratio	0.98(0.06)	0.86(0.03)	0.94(0.01)	0.97(0.03)	
			^{3}NCNO		
CN stretch	3049	2484	2223	2128	
NO stretch	2326	1869	1634	1675	
CN stretch	898	980	945	958	
bend 1	662	601	559	564	
τ	580	480	431	407	
bend 2	277	234	221	219	
ratio	0.83(0.11)	0.94(0.06)		1.00(0.02)	
			CNNO		
CN stretch	2011	2229	2127	2064	
NO stretch	1591	1802	1694	1745	
CN stretch	783	889	835	772	
bend 1	306	599	506	417	
bend 2	152	177	161	180	
τ	127	155	122	94	
ratio	1.16(0.22)	0.90(0.06)		1.08(0.14)	
			TS for CNNO → N_2 + CO		
1	1414			1406	
2	1178			1222	
3	1036			1037	
4	855			928	
5	638			589	
6	−537.8			−517.4	

[a] Vibrational frequencies in cm^{-1}. The quantum chemical estimates are harmonic values obtained for a 6-31G* basis set. [b] Experimental fundamental frequencies from ref 32. [c] Ratios of the experimental frequencies to the quantum chemical frequencies. Where experimental frequencies are not available, the CCSD/6-31G* frequencies take their place in these ratios. Numbers in parentheses denote the variance in these ratios within a given set of data. [d] Experimental fundamental frequencies from ref 34.

representation of eq 1.[35] The reduced matrix procedure of ref 35c is employed, and the energy-transfer rate coefficients are evaluated on the basis of the exponential down model. An energy grain size of 20 cm^{-1} provides numerically converged results for all temperatures studied here with the energies spanning the range from 4000 cm^{-1} below to 4000 cm^{-1} above the threshold.

It is worth recalling the high- and low-pressure limit results for k_{eff} since they provide an important aid in the qualitative interpretation of any modeling. First, in the high-pressure limit $k_{\text{eff}}(T)$ is given by

$$k_{\text{eff}}(T, [M]) = \frac{1}{hQ_{\text{reactants}}(T)}\int \mathrm{d}E\, \mathrm{d}J\, N^{\dagger}_{EJ} \exp(-E/k_{\text{B}}T) \tag{2}$$

where $Q_{\text{reactants}}$ is the partition function for the reactants and $N^{\dagger}_{EJ}$ is the number of available states in the transition state. In contrast, in the limit of low pressure and strong collisions k_{eff} becomes independent of

$$k_{\text{eff}}(T, [M]) = \frac{k_{\text{c}}[M]}{Q_{\text{reactants}}(T)}\int \mathrm{d}E\, \mathrm{d}J\, \rho_{EJ} \exp(-E/k_{\text{B}}T) \tag{3}$$

and instead depends on the product of ρ_{EJ}, the density of states of the complex, with the collision frequency $k_{\text{c}}[M]$.

TABLE 3: Relative Energetics[a]

species	MP2[b]	CCSD[b]	B3LYP[b]	G2[c]	G2(ZPE)[d]	exptl[e]
NCNO	−25 367	−15 877	−19 017	−18 983	−18 187	−17 083
^{3}NCNO	−17 479	−11 042	−17 220	−11 875	−11 004	
CNNO	−16 195	−7 818	−12 023	−11 987	−11 387	
TS	2 812		6 830	6 538	7 065	

[a] Energetics in cm^{-1} relative to infinately separated NC + NO. [b] Quantum chemical estimates employing a 6-31G* basis set and neglecting zero-point energy corrections. [c] G2(MP2) quantum chemical estimates neglecting zero-point energy corrections. [d] Zero-point energy (ZPE) corrected G2(MP2) quantum chemical estimates. Note, in contrast with the standard G2(MP2) procedure, the present ZPE correction is obtained on the basis of the experimental (where available) and CCSD/6-31G* frequencies. [e] Experimental value from ref 9.

The specific procedures employed here in the required evaluations of $Q_{\text{reactant}}(T)$, ρ_{EJ}, k_{c}, and $N^{\dagger}_{EJ}$ are outlined below.

C. $Q_{\text{reactants}}$ and ρ_{EJ}. The reactants partition function is evaluated here on the basis of standard rigid-rotor harmonic-oscillator assumptions. The experimental rotational constants and vibrational frequencies (cf. Table 1) are employed in these evaluations. The use of rigid-rotor harmonic-oscillator assumptions for the reactant partition functions should be satisfactory since the thermal energies of interest here are quite modest (i.e., 100−740 K). The electronic contribution to $Q_{\text{reactants}}$ is incorporated as the factor $2[2 + 2\exp(-173/T)]$, where 173 is the

spin−orbit splitting in K for NO, and the factors of 2 correspond to the electronic degeneracies of CN and the two lowest spin−orbit states of NO.

The effect of anharmonicities on the complex density of states may be more substantial since it is to be evaluated at energies in the neighborhood of the dissociation energy (17 083 cm^{-1}). In earlier work we have estimated an anharmonic correction factor of 1.25 on the basis of diagonal anharmonicity constants.[10] This relatively modest correction factor seems quite reasonable in light of our recent studies suggesting a close similarity between the harmonic and anharmonic state densities for some related molecules.[36] However, there are both additional electronic states and other low-lying local minima on the potential energy surface, which may make further important contributions to the density of states for the complex. The possible importance of the lowest lying triplet state has been alluded to by Sims and Smith in the analysis of their data.[7] Furthermore, a local minimum in the potential arises for a CNNO structure and is at a roughly equivalent energy to the lowest triplet state. This CNNO structure is also directly accessible from reactants.

The contributions that the CNNO and triplet NCNO states make to the overall dynamics depend on the dynamics of the motion between these structures and the singlet NCNO structure. The TS for the isomerization of NCNO to CNNO lies well below the CN + NO asymptote (by 12 500 and 7100 cm^{-1} at the MP2/6-31G* and B3LYP/6-31G* levels, respectively). Also, the NN separation and CN separations for this isomerization transition state are both only about 2.1 Å. Thus, it seems reasonable to assume that there is a rapid interconversion amongst these two isomers. For simplicity we make a similar assumption for the singlet/triplet interconversions. With these assumptions the net effect of these states is simply to increase the effective density of states of the complex.

The results of quantum chemical structural optimizations and vibrational analyses for the singlet and triplet states are reported in Tables 1−3. These data are employed in the estimate of the corresponding state densities owing to the lack of experimental spectroscopic data for these states. Generally, vibrational frequencies obtained at the MP2/6-31G* (or even HF/6-31G*) level provide reasonably satisfactory values for the estimation of state densities. Indeed, the simple multiplicative correction by a factor such as 0.95 is generally expected to provide estimated vibrational frequencies of sufficient accuracy for subsequent kinetic analyses. However, for CN and NO, inordinately small correction factors of 0.72 and 0.49 are required to reproduce the experimental fundamental frequencies.[37] For NCNO a more reasonable average correction factor of 0.98 is obtained at the MP2/6-31G* level. But then for triplet NCNO what appear to be anomalously large frequencies are again obtained for the two highest frequency modes.

These irregularities in the MP2/6-31G* frequencies led us to consider alternative quantum chemical methodologies. We first considered the CISD/6-31G* approach, which does lead to much reduced estimates for the CN and NO stretching frequencies in both the reactants and in triplet NCNO. However, an average correction factor of 0.86 is now required for the NCNO frequencies, indicating once again little consistency in the estimates. The CCSD/6-31G* approach generally provides a much improved estimate of electron correlation effects and was thus considered next. Notably, the average correction factor required for NCNO, CN, and NO is in each case close to 0.95 and has a variance of less than 0.02. Furthermore, the estimated frequencies for triplet NCNO and CNNO seem completely reasonable. Thus, the present kinetic estimates employ the CCSD frequencies wherever experimental estimates are unavailable. The large deviations between the CCSD and MP2 or CISD estimates for each of the species considered here indicates the importance of these higher level estimates. Indeed sample evaluations with the different frequency sets led to variations in the calculated triplet and/or CNNO state densities of typically a factor of 2.

For completeness we have also considered density functional (B3LYP/6-31G*) calculations of these vibrational frequencies since they provide a much less expensive approach than the CCSD (or even MP2) approach and may be as accurate. Comparisons with the experimental and/or CCSD data suggest that the B3LYP/6-31G* approach is indeed quite accurate for the species considered here. The largest deviation arises for the CNNO structure where the B3LYP results are an average of 1.08 times lower than the CCSD frequencies. Notably, the B3LYP estimates for the triplet-state frequencies are in good agreement with the CCSD estimates even though the B3LYP estimated triplet binding energy is clearly in error.

The G2 estimate for the binding energy of NCNO relative to CN + NO is in reasonably satisfactory agreement with the experimental binding energy (cf. Table 3). The G2 estimates for the triplet and CNNO states should similarly be quite reasonable. The 1104 cm^{-1} difference in the G2 versus experimental NCNO binding energies does, however, leave some ambiguity in the choice of reference state for these energies. In the present evaluations, we have chosen the NCNO state as a reference, yielding estimated binding energies of 9901 and 10 284 cm^{-1} for the triplet and CNNO states, respectively. With these binding energies we obtain harmonic-oscillator vibronic state densities at the threshold for producing CN + NO, which are 34% and 46% of the corresponding harmonic-oscillator NCNO density, for the triplet and CNNO states, respectively. We thus employ a net multiplicative correction factor to the harmonic complex density of states of 2.05 (=1.25 + 0.34 + 0.46), corresponding to the sum of these two contributions and the estimated anharmonicity correction mentioned above. Alternatively, one could directly estimate each of the contributions as a function of E and J. However, such an approach was deemed unnecessary here since the total available energy varies only slightly over the thermal energy ranges considered. Interestingly, the energy and nearly angular momentum resolved rate constant data of Zewail and coworkers[9] provides a meaningful test of the accuracy of this estimated state density at the dissociation threshold as described in the next subsection.

D. $N^{\dagger}_{EJ}$ and k_{EJ}. In transition-state theory (TST) the number of available states at the transition state, $N^{\dagger}_{EJ}$, is defined as the minimum in this number over all possible surfaces that separate reactants from products. This minimization typically involves the variation of a single reaction coordinate defining the dividing surfaces. The present evaluations are instead based on a variable reaction coordinate version of transition-state theory in which the minimization is performed with regard to both the definition of the reaction coordinate and the distance.[38−40] In particular, the dividing surfaces are defined by fixing the distance between two arbitrarily chosen fixed points, with one fixed point chosen along the CN axis and the other chosen along the NO axis. Both the distance between the fixed points and the location of each fixed point along its axis are optimized to provide $N^{\dagger}_{EJ}$ in this variable reaction coordinate transition-state theory (VRC-TST) approach.

In related work we have examined the dissociation of NCNO into CN + NO at an energy and angular momentum resolved

level,[10] making comparisons with the corresponding experimental results of Zewail and co-workers.[9] The potential energy surface developed in this earlier work, although perhaps only qualitatively correct, is employed with only minor modifications (described below) in the present evaluations. An important question for this reaction regards the extent of the contribution from the degenerate and nearly degenerate electronic states of CN and NO. The product state distributions observed in the dissociation process suggest that all of these states are accessed in a nearly statistical fashion.[8] However, at closer separations, where the transition state lies at higher energies, the splitting between the electronic states[41] becomes so large that one expects that only the lowest electronic state can make an important contribution to the reactive flux.

In effect there are then two separate bottlenecks to the reactive flux. An outer or phase space theory like transition state occurs at large separations (e.g., 5−10 Å) with an electronic degeneracy g_e^{outer} ranging from 4 to 8

$$g_e^{outer} = 4\left[1 + \frac{N^{\dagger outer}_{E-120(cm^{-1}),J}}{N^{\dagger outer}_{EJ}}\right] \quad (4)$$

and an inner transition state with an electronic degeneracy g_e^{inner} of unity. Assuming that the motion between these two bottlenecks is statistically randomized allows one to write an effective number of states as[42]

$$\frac{1}{N^{\dagger}_{eff}} = \frac{1}{g_e^{outer} N^{\dagger}_{outer}} + \frac{1}{g_e^{inner} N^{\dagger}_{inner}} - \frac{1}{N_{max}} \quad (5)$$

where $N^{\dagger}_{inner}$ and $N^{\dagger}_{outer}$ are the number of available states at the inner and outer transition states, respectively. Meanwhile, N_{max} corresponds to the maximum in the flux between the two transition states. This latter quantity is difficult to evaluate, but it may reasonably be considered to be quite large relative to either $N^{\dagger}_{inner}$ and $N^{\dagger}_{outer}$.[38,40] In this case the last term in eq 5 may be neglected. Sample calculations suggest that more precise evaluations of N_{max} would not qualitatively affect the present results.

Here, we implement $N^{\dagger}_{eff}$ with $N_{max} = \infty$ as our approximation to the transition-state number of states. The outer transition state number of states is evaluated on a grid of separations ranging from 5 to 10 Å employing a center-of-mass separation distance as the reaction coordinate. The inner transition-state number of states is evaluated for a bond length reaction coordinate on a grid of separations ranging from 2.4 to 3.6 Å. Previous full optimizations of the reaction coordinate within the present VRC-TST scheme generally provided only a minor reduction of about 10% or less in the estimate for $N^{\dagger}_{inner}$.[38] This reduction is not applied here.

The photodissociation experiments of Zewail and co-workers provide explicit values for the energy-resolved dissociation rate constant as a function of energy.[9] Furthermore, the reactant NCNO is cooled down to a few K in these experiments via a supersonic expansion, thereby greatly restricting the range of J. A comparison of the present theoretical predictions for the dissociation rate constant, employing a typical J value of 3, with the experimental rate constants is provided in Figure 2.[43] At the lowest energies the outer transition state is expected to dominate the kinetics. Furthermore, the evaluation of the number of states at large separations is essentially independent of the potential. As a result, the good agreement between the theoretical predictions and the experimental observations in the near threshold region, where there is little flexibility in the $N^{\dagger}_{eff}$ estimates, suggests that the present estimate for the density of states of the complex is quite accurate.

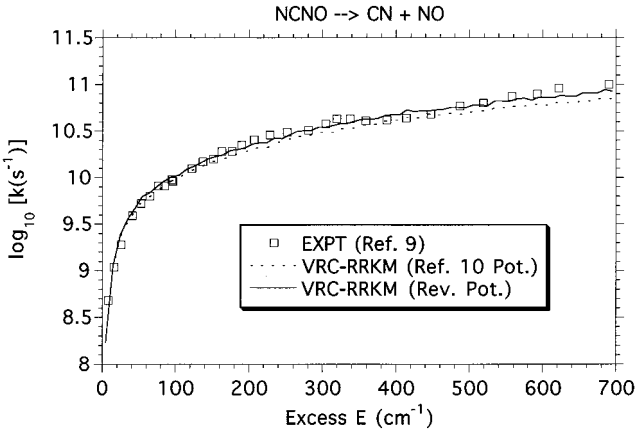

Figure 2. Plot of the microscopic rate as a function of excess energy for the dissociation of NCNO. Squares denote the experimental data of ref 9. Solid and dashed lines denote the present variable reaction coordinate transition-state theory results employing the original[10] and modified model potentials, respectively, and are for $J = 3$.

At higher energies the interplay between the inner and outer transition state becomes important. The calculations employing the model potential of ref 10 are seen to somewhat understimate the observed rate constant in this region. This model potential was obtained on the basis of empirical considerations, and so modest variations in its parameters are reasonable. Sample calculations employing an effective β parameter for the Varshni potential of 0.46 Å^2 (instead of 0.517) and an orientational modulation of the bonding potential according to the square root of $[\cos(\Delta\theta)]$ (instead of the square) were also performed. As seen in Figure 2 these calculations provide a markedly improved agreement at the higher energies while retaining the good agreement near the thresholds. This modified potential was thus employed in the subsequent evaluations of the transition-state number of states and thereby the thermal association rate constant.

E. Collisional Parameters. As is standard practice a Lennard-Jones model for the collisional frequency, k_c, of Ar with NCNO was employed (cf. eqs 5.5.14 and 5.5.17 of ref 35). The Ar···NCNO Lennard-Jones parameters $\sigma = 3.9$ Å and $\epsilon = 205$ K were obtained from the data given in ref 44 for Ar and the roughly analogous NCCN species. Unfortunately, there are no simple a priori means for estimating the average energy transfer $\langle\Delta E\rangle$. Thus, we present results for the temperature and pressure dependence of the predicted effective rate constants for $\langle\Delta E\rangle_{down}$ values ranging from −25 to −800 cm^{-1} and employ the simple exponential down model.

IV. Results and Discussion

A. Experimental Results. The rate constant of the CN + NO reaction was determined by measuring the decay of CN LIF signals under pseudo-first-order conditions with [NO] ≫ [CN] over a wide range of temperature (207−740 K) and total pressure (30−900 Torr) using Ar as the diluent. The effects of pressure, measured at 704, 430, 297, and 207 K, are presented in Table 4 and illustrated in Figures 3 and 4. These experimental rate constants are estimated to have error bars of about ±20%. In Figures 3 and 4, the results of Sims and Smith,[7] obtained at 450, 296, and 205 ± 2 K, are also included. Two additional sets of data obtained at 145 and 102 K by Sims and Smith are presented in Figure 5. These results reveal an

TABLE 4: Experimental Rate Constants for CN + NO

$T = 207$ K		$T = 297$ K		$T = 430$ K		$T = 740$ K	
P^a	k^b	P	k	P	k	P	k
30	3.93	30	1.35	50	0.65	100	0.26
30	3.02	51	2.01	74	0.90	100	0.28
50	5.89	100	3.45	100	1.30	100	0.30
65	7.43	100	3.33	100	1.23	200	0.44
100	8.64	100	3.39	100	1.31	275	0.55
100	8.11	101	3.39	202	2.02	350	0.66
101	9.09	101	3.65	300	2.85	425	0.76
125	10.1	151	4.95	360	3.13	500	1.02
150	12.8	225	5.73	400	3.43	500	0.95
150	11.9	300	7.60	450	3.83	600	1.08
200	15.1	400	7.72	502	4.36	600	1.11
250	14.9	498	8.91	599	4.79	702	1.23
300	17.8	498	10.8	652	4.82	800	1.46
400	20.3	501	11.0	698	5.22		
500	24.0	501	9.61	752	5.43		
500	20.3	646	10.8	800	5.57		
600	22.4	649	10.5				
605	22.6	901	12.4				
700	21.0						
700	19.9						
700	25.1						
700	24.2						
800	21.8						
805	23.1						
809	28.5						
810	20.8						

[a] Pressure in units of Torr. [b] Rates constants are in units of 10^{-12} cm^3 s^{-1} and have estimated error bars of ± 20%.

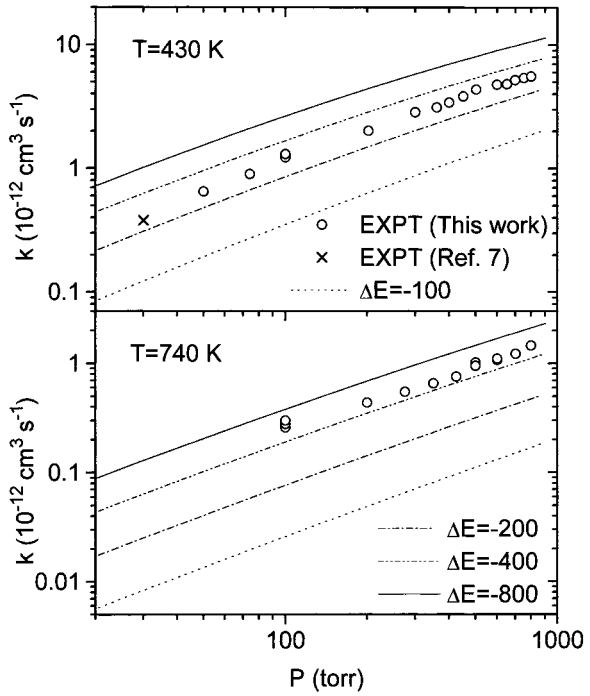

Figure 3. Plot of the pressure dependence of the CN + NO association rate constant for temperatures of 430 and 740 K. The circles denote the present experimental results. The cross denotes the experimental data of Sims and Smith.[7] The solid, dashed−dashed dotted, dashed−dotted, and dotted lines denote the present theoretical predictions employing $\langle \Delta E \rangle_{down}$ values of −800, −400, −200, and −100 cm^{-1}, respectively.

extensive pressure dependence of the bimolecular rate constant below 900 Torr, the highest pressure reported in the studies.

In order to estimate the limiting values of the association rate constants at high and low pressures, k^∞ and k^0 [which relate directly to the nature of the transition state involved in the

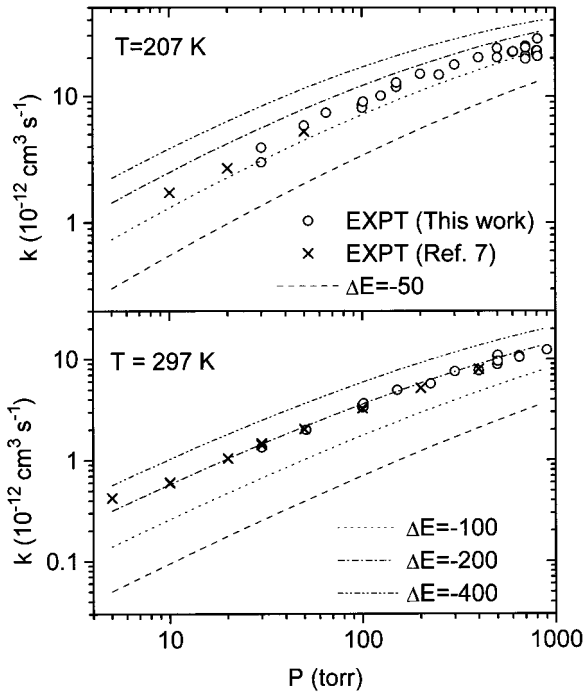

Figure 4. As in Figure 3, but for temperatures of 207 and 297 K. The dahsed line corresponds to $\langle \Delta E \rangle_{down} = -50$ cm^{-1}.

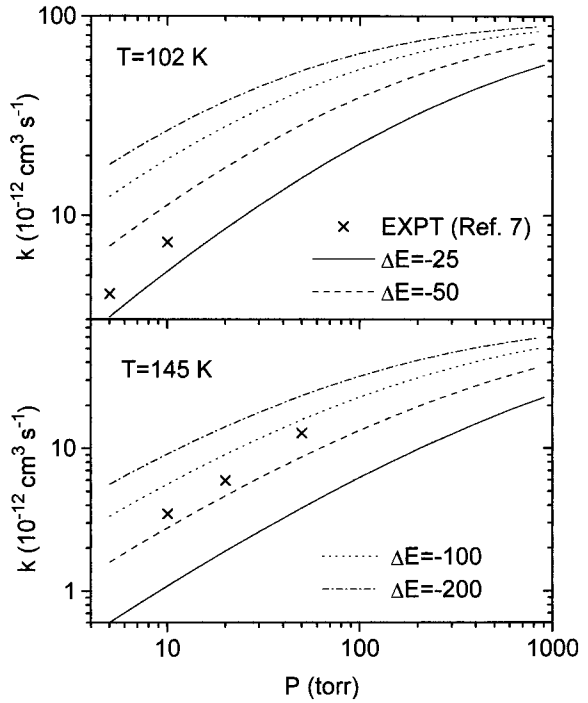

Figure 5. As in Figure 4, but for temperatures of 102 and 145 K. The solid line now corresponds to $\langle \Delta E \rangle_{down} = -25$ cm^{-1}.

association step and the efficiency of energy transfer from the excited NCNO to the third-body (M), respectively], we extrapolated the pressure-dependent data with Troe's method using the following empirical equations[45,46]

$$k = a[b/(1 + b)]F \tag{6}$$

$$\log F = \log F_c/[1 + (\log b)^2] \tag{7}$$

where $a = k^\infty$, $b = k^0[M]/k^\infty$, and F_c is a fitting parameter (typically 0.6 ± 0.1) that accounts for the broadening of the pressure fall-off curve.[45,46] Least-squares analyses of the

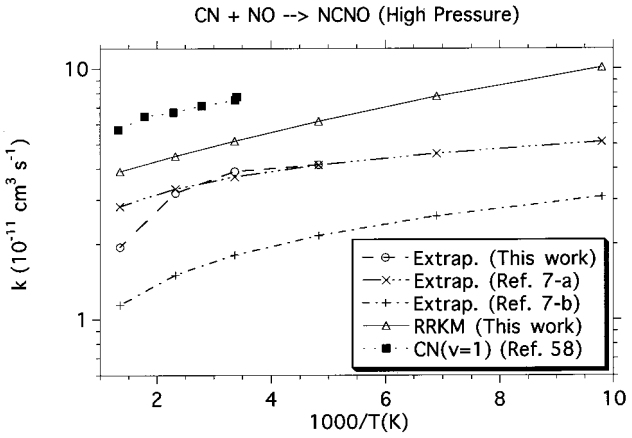

Figure 6. Plot of the temperature dependence for the high-pressure limiting thermal association rate constant. The filled squares denote the CN vibrational relaxation data of Sims and Smith,[43] the circles denote the Troe-based extrapolations of the present work, the crosses and pluses denote the corresponding extrapolations of Sims and Smith,[7] and the triangles denote the present RRKM estimates. The lines are provided as a guide to the eye.

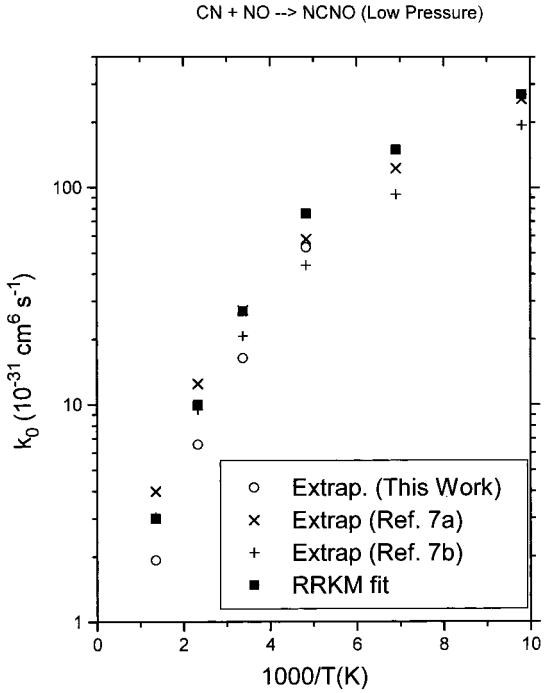

Figure 7. Plot of the temperature dependence of the low-pressure limiting thermal association rate constant. The circles, pluses, and crosses are as in Figure 6. The filled squares denote the present RRKM estimates employing at each temperature the $\langle \Delta E \rangle_{down}$ value that provides the best fit to the observed pressure dependence (cf. Figures 3−5).

experimental data shown in Figures 3 and 4 with the above equations using $F_c = 0.6$ gave rise to the limiting values of k^∞ and k^0, which are summarized in Figures 6 and 7, respectively. For most temperatures, increasing F_c by 0.1 yields about a 40% decrease in k^∞ and about a 3% decrease in k^0. For $T = 207$ K such an increase in F_c instead yields only an 7% decrease in k^∞ and an 18% decrease in k^0.

Also included in Figures 6 and 7 are the extrapolated results of Sims and Smith employing similar extrapolation techniques (in which the fitting parameters for the pressure fall-off were estimated separately).[7] These rate constants and the pressure dependency depicted in Figures 3−5 are compared below with theoretically predicted results.

B. Comparison of Theory and Experiment. The pressure dependence of the theoretically predicted association rate constants k_{eff} are compared with both the present experimental data and the prior experimental data of ref 7 in Figures 3−5, for temperatures of 740, 430, 297, 207, 145, and 102 K. Some of the experimental data of Sims and Smith[7] corresponds to a slightly different temperature from that plotted, but only minor corrections would be expected. The data of ref 7 and the present experimental data are in remarkably good agreement in the regions of their overlap. This agreement provides strong support for the accuracy of both sets of data.

For each temperature the predicted and observed pressure dependencies are seen to be in satisfactory agreement. Notably, the average energy-transfer parameter $\langle \Delta E \rangle_{down}$, which provides this agreement, decreases quite substantially with decreasing temperature. The best fit values are about −500, −300, −200, −140, −70, and −35 cm^{-1} for temperatures of 740, 430, 297, 207, 145, and 102 K, respectively. A slight increase in $\langle \Delta E \rangle_{down}$ with increasing temperature is perhaps to be expected given the increasing average collision energy. However, the magnitude of this increase (and of the actual values at the highest temperatures) are so large as to be suggestive of some failure in the theoretical model, perhaps related to the treatment of the angular momentum dependence of either the dissociation rate constants or the energy-transfer process. It would be interesting to examine such possibilities in future studies.

In Figure 6 a plot of the temperature dependence of the high-pressure limiting rate constant is provided. Consideration of the TST values presented therein suggests that the high-pressure limit is never closely approached in the present experiments. The closest approach is for a temperature of 207 K where the experimental data at a pressure of 800 Torr is only 2.5 times lower than the TST estimated high-pressure rate constant. In this instance it is difficult to accurately extrapolate the experimental data to the high-pressure limit and it is not surprising that the experimental extrapolations are not in good agreement with the theoretical estimates.

An alternative indirect experimental measure of the high-pressure rate constants is provided by the experiments of Sims and Smith, which probe the rate of vibrational relaxation of CN in $v = 1$ arising from collisions with NO.[47] This relaxation rate would be expected to correlate quite closely with the rate of complex formation and thus with the high-pressure limiting rate constant. These experimental relaxation rate constants are also plotted in Figure 6 and are about 40% higher than the theoretical estimates. This reasonably minor discrepancy again may be an indication of errors in the treatment of angular momentum effects for the transition state. Notably, a theoretical model that yields a somewhat greater high-pressure rate constant at the higher temperatures (in agreement with these relaxation rate constants) would also require somewhat smaller energy-transfer parameters at higher temperatures.

The temperature dependence of the various estimates for the low pressure limiting rate constant is illustrated in Figure 7. In this instance, the TST results for the fitted average energy-transfer coefficients are seen to be in good agreement with those obtained from the present Troe-based extrapolations of the experimental data. The similar extrapolations of ref 7 predict only slightly higher rates.

V. Concluding Remarks

The good agreement between the present experimental results and those of Sims and Smith[7] where the two experiments overlap

demonstrates the validity of both experiments. The implementation of the Troe factorization method provides an estimate for the high-pressure rate constant ($k = 6.16 \times 10^{-7} T^{-1.50} \exp(-332/T)$ cm^3 s^{-1}), which is essentially identical to that obtained by Sims and Smith.[7] The expression $k = 3.4 \times 10^{-10} \exp(120/T)$ cm^3 s^{-1} provides a good representation of the transition-state theory estimates for the high-pressure rate constant in the 207−740 K region.

The theoretical study suggests the importance of anharmonic effects and of the secondary CNNO association channel in yielding a net increase in the density of states by a factor of about 2. The variational RRKM results employing a simple model potential provide a completely satisfactory description of the experimental results for both the dissociation and the association. The agreement for the association results relies upon fitted values for $\langle \Delta E \rangle_{\text{down}}$ that decrease in magnitude from −500 to −35 cm^{-1} from $T = 740$ to 102 K.

Acknowledgment. S.J.K. acknowledges the support of this research through NSF Grant CHE-9423725 and through an Emerson fellowship from the Cherry Emerson Center at Emory University. S.K. and M.C.L. acknowledge the support of this work by the Caltech Multidisciplinary University Research Initiative under Office of Naval Research Grant No. NOOO14-951-1338. We thank the Cherry Emerson Center for Scientific Computation for the use of computing facilities and various programs.

References and Notes

(1) Melius, C. F. *25th JANNAF Combustion Meeting (Proceedings)*; 1988; Vol. II, pp 155−62.

(2) Melius, C. F. *Philos. Trans. R. Soc. London A* **1992**, 339−365.

(3) He, Y.; Wu, C. H.; Lin, M. C.; Melius, C. F. *Schock Waves @ Marseille*; Brown, R., Dumitrescu, L. Z., Eds.; Springer-Verlag: Bein Heidelberg, 1995; pp 89−94.

(4) Colket, M. B. *Int. J. Chem. Kinet.* **1984**, *16*, 353.

(5) Natarajan, K.; Roth, P. *Symp. (Int.) Combust. (Proc.)* **1986**, *21*, 729.

(6) Wang, N. S.; Yang, D. L.; Lin, M. C. *Chem. Phys. Lett.* **1989**, *163*, 484.

(7) Sims, I. R.; Smith, I. W. M. *J. Chem. Soc., Faraday Trans.* **1993**, *89*, 1.

(8) Nadler, I.; Noble, M.; Reisler, H.; Wittig, C. *J. Chem. Phys.* **1985**, *82*, 2608. Qian, C. X. W.; Noble, M.; Nadler, I.; Reisler, H.; Wittig, C. *J. Chem. Phys.* **1985**, *83*, 5573. Reisler, H.; Wittig, C. *Annu. Rev. Phys. Chem.* **1986**, *37*, 307. Qian, C. X. W.; Ogai, A.; Reisler, H.; Wittig, C. *J. Chem. Phys.* **1989**, *90*, 209.

(9) Khundkar, L. R.; Knee, J. L.; Zewail, A. H. *J. Chem. Phys.* **1987**, *87*, 77.

(10) Klippenstein, S. J.; Khundkar, L. R.; Zewail, A. H.; Marcus, R. A. *J. Chem. Phys.* **1988**, *89*, 4761.

(11) Yang, D. L.; Lin, M. C. In *The Chemical Dynamics and Kinetics of Small Molecules*; Liu, K., Wagner, A. F., Eds.; World Scientific: River Edge, NJ, 1996; Vol. I, pp 164−213.

(12) Szabo, A.; Ostlund, N. S. *Modern Quantum Chemistry: Introduction to Advanced Electronic Structure Theory*; McGraw-Hill: New York, 1982.

(13) Hehre, W. J.; Radom, L.; Schleyer, P. V. R.; Pople, J. A. *Ab Initio Molecular Orbital Theory*; Wiley-Interscience: New York, 1986.

(14) Møller, C.; Plesset, M. S. *Phys. Rev.* **1934**, *46*, 618.

(15) Pople, J. A.; Binkley, J. S.; Seeger, R. *Int. J. Quantum Chem. Symp.* **1976**, *10*, 1.

(16) Krishnan, R.; Pople, J. A. *Int. J. Quantum Chem.* **1978**, *14*, 91.

(17) Krishnan, R.; Schlegel, H. B.; Pople, J. A. *J. Chem. Phys.* **1980**, *72*, 4654.

(18) Raghavachari, K.; Pople, J. A. *Int. J. Quantum Chem.* **1981**, *20*, 167.

(19) Cizek, J. *Adv. Chem. Phys.* **1969**, *14*, 35.

(20) Bartlett, R. J. *Annu. Rev. Phys. Chem.* **1981**, *32*, 359. Purvis, G. D.; Bartlett, R. J. *J. Chem. Phys.* **1982**, *76*, 1910.

(21) Paldus, J. In *New Horizons of Quantum Chemistry*; Löwdin, P.-O., Pullman, B., Eds.; Reidel: Dordrecht, 1983; p 31.

(22) Bartlett, R. J.; Dykstra, C. E.; Paldus, J. In *Advanced Theories and Computational Approaches to the Electronic Structure of Molecules*; Dykstra, C. E., Ed.; Reidel: Dordrecht, 1984; p 127.

(23) Scuseria, G. E.; Scheiner, A. C.; Lee, T. J.; Rice, J. E.; Schaefer, H. F., III. *J. Chem. Phys.* **1987**, *86*, 2881.

(24) Scheiner, A. C.; Scuseria, G. E.; Rice, J. E.; Lee, T. J.; Schaefer, H. F., III. *J. Chem. Phys.* **1987**, *87*, 5361.

(25) Parr, R. G.; Yang, W. *Density-Functional Theory of Atoms and Molecules*; Oxford: Oxford, 1989.

(26) Labanowski, J. K., Andzelm, J. W., Eds. *Density Functional Methods in Chemistry*; Springer-Verlag: New York, 1991.

(27) Becke, A. D. *J. Chem. Phys.* **1993**, *98*, 5648; *Ibid.* **1992**, *97*, 9173; *Ibid.* **1992**, *96*, 2155; *Ibid.* **1988**, *88*, 1053. Lee, C.; Yang, W.; Parr, R. G. *Phys. Rev. B* **1988**, *37*, 785.

(28) Curtiss, L. A.; Raghavachari, K.; Pople, J. A. *J. Chem. Phys.* **1993**, *98*, 1293.

(29) Curtiss, L. A.; Raghavachari, K.; Trucks, G. W.; Pople, J. A. *J. Chem. Phys.* **1991**, *94*, 7221.

(30) Durant, J. L., Jr.; Rohlfing, C. M. *J. Chem. Phys.* **1993**, *98*, 8031.

(31) Frisch, M. J.; Trucks, G. W.; Head-Gordon, M.; Gill, P. M. W.; Wong, M. W.; Foresman, J. B.; Johnson, B. G.; Schlegel, H. B.; Robb, M. A.; Replogle, E. S.; Gomperts, R.; Andres, J. L.; Raghavachari, K.; Binkley, J. S.; Gonzalez, C.; Martin, R. L.; Fox, D. J.; Defrees, D. J.; Baker, J.; Stewart, J. J. P.; Pople, J. A. *Gaussian 92/DFT*, Revision G.1; Gaussian Inc.: Pittsburgh, PA, 1992.

(32) *Landolt-Börnstein, Physical Constants for Atoms and Molecules*; Springer: Berlin, 1983; Part II (Suppl.).

(33) Dickinson, R.; Kirby, G. W.; Sweeny, J. G.; Tyler, J. K. *J. Chem. Soc., Faraday Trans.* **1978**, *74*, 1393.

(34) Bak, B.; Nicolaisen, F. M.; Nielsen, O. J. *J. Mol. Struct.* **1979**, *51*, 17.

(35) Gilbert, R. G.; Smith, S. C. *Theory of Unimolecular Recombination Reactions*; Blackwell Scientific: Oxford, 1990. (b) Holbrook, R. A.; Pilling, M. J.; Robertson, S. H. *Unimolecular Reactions*, 2nd edition; Wiley: Chichester, 1996. (c) Robertson, S. H.; Pilling, M. J.; Baulch, D. L.; Green, N. J. B. *J. Phys. Chem.* **1995**, *99*, 13452.

(36) Klippenstein, S. J. *J. Phys. Chem.* To be submitted.

(37) Strictly speaking we should compare the harmonic frequencies with the corresponding harmonic experimental frequencies. However, the anharmonicities for CN and NO are both quite small (13.1 and 14.1 cm-1, respectively) and so are of negligible importance in considering the large deviations between the experimental and theoretical estimates. One may expect the anharmonicities in NCNO, which are unknown, to be of a similarly minor importance in such comparisons.

(38) Klippenstein, S. J. *Chem. Phys. Lett.* **1990**, *170*, 71; *J. Chem. Phys.* **1991**, *94*, 6469; **1992**, *96*, 367.

(39) Klippenstein, S. J. In *The Chemical Dynamics and Kinetics of Small Radicals*; Liu, K., Wagner, A. F., Eds.; World Scientific: River Edge, NJ, 1996.

(40) Klippenstein, S. J. *J. Phys. Chem.* **1994**, *98*, 11459.

(41) Bai, Y. Y.; Segal, G. A. *Chem. Phys. Lett.* **1988**, *151*, 31.

(42) Hirschfelder, J. O.; Wigner, E. *J. Chem. Phys.* **1939**, *7*, 616. Miller, W. H.; *J. Chem. Phys.* **1976**, *65*, 2216. Chesnavich, W. J.; Bass, L.; Su, T.; Bowers, M. T. *J. Chem. Phys.* **1981**, *74*, 2228. Rai, S. N.; Truhlar, D. G. *J. Chem. Phys.* **1983**, *79*, 6046.

(43) A thermal average over the reactant rotational states could have been performed in the theoretical analysis. However, the variation of the rate constant with J in this low J limit essentially reduces to an uncertainty in the dissociation threshold corresponding to the thermal rotational energy of the reactants. In this case, this uncertainty corresponds to only a few cm^{-1} in the energy scale of Figure 2 and so was deemed unimportant.

(44) Hirschfelder, J. O.; Curtiss, C. F.; Bird, R. B. *Molecular Theory of Gases and Liquids*; 4th printing; Wiley: New York, 1967.

(45) Troe, J. *J. Phys. Chem.* **1979**, *83*, 114.

(46) Troe, J. *Ber. Bunsenges. Phys. Chem.* **1983**, *87*, 161. Gilbert, R. G.; Luther, K.; Troe, J. *Ber. Bunsen-Ges. Phys. Chem.* **1983**, *87*, 169.

(47) Sims, I. R.; Smith, I. W. M. *J. Chem. Soc., Faraday Trans. 2* **1988**, *84*, 527.